Temperature and gain tuning of plasmonic coherent perfect absorbers

Myoung Jin Jung,[1] Choloong Han,[1] Jae Woong Yoon,[1,2] and Seok Ho Song[1,*]

[1]*Department of Physics, Hanyang University, Seoul 133-791, South Korea*
[2]*jaeong.yoon@gamil.com*
[*]*shsong@hanyang.ac.kr*

Abstract: We experimentally demonstrate temperature-tuned and gain-assisted surface-plasmonic coherent perfect absorbers. In these devices, coherent perfect absorption (CPA) is supported by balancing the absorber's radiative and non-radiative decay rates under thermal tuning of free-electron collision frequency in the Ag layer and optical tuning of the amplification rate in the adjacent dielectric film with optical gain, respectively. The results show that these methods are experimentally feasible and applicable to various CPA configurations.

OCIS codes: (030.1670) Coherent optical effects; (240.6680) Surface plasmons; (300.1030) Absorption.

References and links

1. Y. D. Chong, L. Ge, H. Cao, and A. D. Stone, "Coherent perfect absorbers: time-reversed lasers," Phys. Rev. Lett. **105**(5), 053901 (2010).
2. W. Wan, Y. Chong, L. Ge, H. Noh, A. D. Stone, and H. Cao, "Time-reversed lasing and interferometric control of absorption," Science **331**(6019), 889–892 (2011).
3. J. Yoon, K. H. Seol, S. H. Song, and R. Magnusson, "Critical coupling in dissipative surface-plasmon resonators with multiple ports," Opt. Express **18**(25), 25702–25711 (2010).
4. J. Zhang, K. F. McDonald, and N. I. Zheludev, "Controlling light-with-light without nonlinearity," Light Sci. Appl. **1**(7), e18 (2012).
5. R. Bruck and O. L. Muskens, "Plasmonic nanoantennas as integrated coherent perfect absorbers on SOI waveguides for modulators and all-optical switches," Opt. Express **21**(23), 27652–27671 (2013).
6. T. Roger, S. Vezzoli, E. Bolduc, J. Valente, J. J. F. Heitz, J. Jeffers, C. Soci, J. Leach, C. Couteau, N. I. Zheludev, and D. Faccio, "Coherent perfect absorption in deeply subwavelength films in the single-photon regime," Nat. Commun. **6**, 7031 (2015).
7. X. Fang, M. L. Tseng, J. Y. Ou, K. F. MacDonald, D. P. Tsai, and N. I. Zheludev, "Ultrafast all-optical switching via coherent modulation of metamaterial absorption," Appl. Phys. Lett. **104**(14), 141102 (2014).
8. J. W. Yoon, G. M. Koh, S. H. Song, and R. Magnusson, "Measurement and modeling of a complete optical absorption and scattering by coherent surface plasmon-polariton excitation using a silver thin-film grating," Phys. Rev. Lett. **109**(25), 257402 (2012).
9. S. Feng and K. Halterman, "Coherent perfect absorption in epsilon-near-zero metamaterials," Phys. Rev. B **86**(16), 165103 (2012).
10. J. A. Giese, J. W. Yoon, B. R. Wenner, J. W. Allen, M. S. Allen, and R. Magnusson, "Guided-mode resonant coherent light absorbers," Opt. Lett. **39**(3), 486–488 (2014).
11. S. M. Rao, J. J. F. Heitz, T. Roger, N. Westerberg, and D. Faccio, "Coherent control of light interaction with graphene," Opt. Lett. **39**(18), 5345–5347 (2014).
12. M. Pu, Q. Feng, M. Wang, C. Hu, C. Huang, X. Ma, Z. Zhao, C. Wang, and X. Luo, "Ultrathin broadband nearly perfect absorber with symmetrical coherent illumination," Opt. Express **20**(3), 2246–2254 (2012).
13. S. Li, J. Luo, S. Anwar, S. Li, W. Lu, Z. H. Hang, Y. Lai, B. Hou, M. Shen, and C. Wang, "Broadband perfect absorption of ultrathin conductive films with coherent illumination: super performance of microwave radiation," Phys. Rev. B **91**(22), 220301 (2015).
14. J. W. Yoon, M. J. Jung, and S. H. Song, "Gain-assisted critical coupling for high-performance coherent perfect absorbers," Opt. Lett. **40**(10), 2309–2312 (2015).
15. J. Chandezon, M. Dupuis, G. Cornet, and D. Maystre, "Multicoated gratings: a differential formalism applicable in the entire optical region," J. Opt. Soc. Am. **72**(7), 839–846 (1982).
16. E. D. Palik, *Handbook of Optical Constants of Solids* (Academic, 1985).
17. J. Yoon, S. H. Song, and J.-H. Kim, "Extraction efficiency of highly confined surface plasmon-polaritons to far-field radiation: an upper limit," Opt. Express **16**(2), 1269–1279 (2008).
18. P. D. Pathak and N. P. Shah, "Debye temperature of silver and aluminum at high temperatures – some new correlations," Phys. Status Solidi A. **55**(2), K159–K162 (1979).

#242474 Received 10 Jun 2015; revised 16 Jul 2015; accepted 17 Jul 2015; published 22 Jul 2015

19. J. A. McKay and J. A. Rayne, "Temperature dependence of the infrared absorptivity of the noble metals," Phys. Rev. B **13**(2), 673–685 (1976).
20. X. Li, Z. Cao, Q. Shen, and Y. Yang, "Influence of dopant concentration on thermos-optic properties of PMMA composite," Mater. Lett. **60**(9–10), 1238–1241 (2006).
21. I. De Leon and P. Berini, "Modeling surface plasmon-polariton gain in planar metallic structures," Opt. Express **17**(22), 20191–20202 (2009).
22. W. L. Barnes, "Fluorescence near interfaces: the role of photonic mode density," J. Mod. Opt. **45**(4), 661–699 (1998).
23. J. Zhang, C. Guo, K. Liu, Z. Zhu, W. Ye, X. Yuan, and S. Qin, "Coherent perfect absorption and transparency in a nanostructured graphene film," Opt. Express **22**(10), 12524–12532 (2014).
24. J. R. Piper and S. Fan, "Total absorption in a graphene monolayer in the optical regime by critical coupling with a photonic crystal guided resonance," ACS Photonics **1**(4), 347–353 (2014).
25. C. M. Bender and S. Boettcher, "Real spectra in non-Hermitian Hamiltonians having PT symmetry," Phys. Rev. Lett. **80**(24), 5243–5246 (1998).
26. Z. Lin, H. Ramezani, T. Eichelkraut, T. Kottos, H. Cao, and D. N. Christodoulides, "Unidirectional invisibility induced by PT-symmetric periodic structures," Phys. Rev. Lett. **106**(21), 213901 (2011).
27. L. Feng, Z. J. Wong, R.-M. Ma, Y. Wang, and X. Zhang, "Single-mode laser by parity-time symmetry breaking," Science **346**(6212), 972–975 (2014).

1. Introduction

Interference of electromagnetic fields is a key property in many coherent optical systems for surface metrology, infrared spectroscopy, biomedical imaging, and optical communication networks. Recently, a new class of interferometric optical systems was proposed on the basis of a time-reversed laser concept, so-called coherent perfect absorption (CPA) [1–3]. In CPA elements, incident optical fields can be either completely absorbed or totally scattered by controlling the phases of incoming fields while maintaining the resonator's intrinsic properties unchanged. Utilizing this intriguing linear optical effect, theoretical and experimental proposals have showed that this phenomenon provides unique opportunities for optical coherence filters and compact all-optical modulators and switches in low-power and high-speed operation regimes [4–7].

Various CPA configurations to exploit this effect for active device applications have been investigated. In the first proposal [1,2], silicon Fabry-Pérot cavities were used in proof-of-concept experiments. The proposal triggered extensive study of more advanced CPA element designs enabled by surface-plasmon resonances [3,8], metamaterials [4,9], guided-mode resonances [10], resonant photonic thin films with graphene monolayers [9–11], and many others. More recently, the CPA concept is further extended to efficient broadband absorbers operating with nonresonant field interference in ultra-thin heavily doped Si films in the infrared spectral domain [12] and metallic films in the microwave regions [13]. In these systems, obtaining strictly perfect coherent absorption and the maximal signal extinction ratio requires the critical coupling condition where the resonator's radiative (γ_{rad}) and non-radiative (γ_{nr}) decay rates are identical. To realize a CPA element with the desired performance in practice, it is important for the element to allow feasible methods of fine-tuning for accessing the critical coupling condition.

As a possible solution to this problem, we theoretically proposed gain-assisted critical coupling, which permits all-optical continuous tuning of γ_{nr} without altering the absorber's geometrical parameters [14]. In this paper, we experimentally study two separate tuning methods for continuously accessing the critical coupling condition. They are temperature-tuned and gain-tuned critical coupling schemes. Using a surface-plasmon-resonance grating structure loaded with an optical gain medium, we design, fabricate, and test the proposed tunable CPA elements. We confirm that the temperature and gain tuning methods are experimentally feasible for surface-plasmonic CPA elements.

2. Optimal structures for tunable CPAs

We consider a surface-plasmon-polariton (SPP) resonance coherent absorber consisting of an Ag grating and a dye-doped PMMA over-layer, as shown in Fig. 1(a). In this structure, phase-sensitive light absorption is obtained for single SPP mode coupling with two external planewaves at different diffraction orders. In our case, two incoming planewaves with

#242474 Received 10 Jun 2015; revised 16 Jul 2015; accepted 17 Jul 2015; published 22 Jul 2015

amplitudes a_1 and a_2 simultaneously excite a single SPP mode through first- and second-order diffraction processes, respectively. Two outgoing amplitudes, b_1 and b_2, are determined by the amplitude of the excited SPP mode and its first- and second-order diffraction amplitudes. Therefore, the angles θ_1 and θ_2 of incidence satisfy the phase matching condition

$$k_0 \sin\theta_m = k_{SP} - 2\pi m / \Lambda \,, \tag{1}$$

where k_0 is the vacuum wave number of the incident planewave, k_{SP} denotes the in-plane wave vector of the SPP mode, and Λ is the period of the Ag grating. A good CPA element requires optimal radiative and non-radiative decay rates of its operating resonance mode and also optimal intensity ratios between coherent incoming beams.

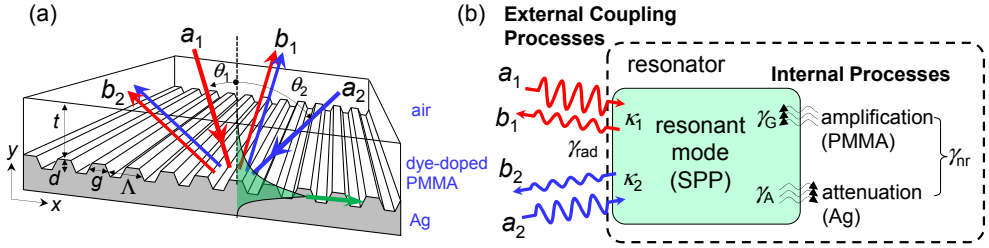

Fig. 1. Surface-plasmon resonance grating structure for a CPA element. (a) Schematic of the structure and light coupling configuration. (b) Two-port resonator model describing the system illustrated in (a).

Essence of the proposed coupling configuration and associated phase-sensitive resonant absorption can be described by the two-port resonator model shown in Fig. 1(b). In this model, a pair of incoming and outgoing planewaves with respective amplitudes a_m and b_m at θ_m is assigned to coupled radiation port m (= 1 or 2) and its coupling constant with the SPP mode is κ_m. The amplitudes a_m and b_m are normalized such that their absolute squares $|a_m|^2$ and $|b_m|^2$ respectively represent incoming and outgoing powers at port m. To include stimulated emission in the dye-doped PMMA layer and ohmic absorption in the Ag region, the non-radiative decay rate γ_{nr} of the SPP mode is given by $\gamma_{nr} = \gamma_A - \gamma_G$, where γ_A is the attenuation rate due to ohmic absorption in Ag and γ_G is the amplification rate due to the optical gain in PMMA. We use this model to identify essential requirements for high-performance CPA operation. Applying the temporal coupled-mode theory of dissipative resonators [3] to the model system, the net absorbance under coherent light incidence is written by the following expression

$$A_{net} = \frac{4(\gamma_A - \gamma_G)\gamma_{rad}}{(\omega-\omega_0)^2 + (\gamma_{rad} + \gamma_A - \gamma_G)^2} \frac{\eta_1 I_1 + \eta_2 I_2 + 2\sqrt{\eta_1\eta_2 I_1 I_2}\cos(\phi+\phi_0)}{I_1 + I_2}, \tag{2}$$

where $\eta_m = |\kappa_m|^2/(|\kappa_1|^2 + |\kappa_2|^2)$ is the normalized coupling strength at the radiation port m, $I_m = |a_m|^2$ is the incoming power at port m, $\phi = \arg(a_1) - \arg(a_2)$ is the incident phase-difference, and $\phi_0 = \arg(\kappa_1) - \arg(\kappa_2)$ is the coupling phase-difference. Conditions for the two special cases of the CPA state, $A_{net} = 1$, and total scattering state, $A_{net} = 0$, are readily found from Eq. (2).

First, the CPA state requires two independent conditions: $\gamma_{rad} = \gamma_{nr} = \gamma_A - \gamma_G$ and $I_1/I_2 = \eta_1/\eta_2$. The former is referred to as the *critical coupling condition*. Once the absorber design and the incoming wave intensities satisfy these conditions, the peak absorbance at $\omega = \omega_0$ is given by

$$A_{net}(\omega_0) = 1 - 2\eta_1\eta_2\left[1 - \cos(\phi+\phi_0)\right]. \tag{3}$$

Obviously, $A_{net} = 1$ for $\phi + \phi_0 = 2q\pi$, where q is an integer. This CPA state results from the constructively built SPP field and associated destructive interference simultaneously

#242474 Received 10 Jun 2015; revised 16 Jul 2015; accepted 17 Jul 2015; published 22 Jul 2015

occurring for both b_1 and b_2. When the SPP fields separately excited by a_1 and a_2 cancel each other for $\phi + \phi_0 = (2q + 1)\pi$, i.e., $\cos(\phi + \phi_0) = -1$, the net absorbance is minimized to $1–4\eta_1\eta_2$. Note that this minimal absorbance is not necessarily 0 but vanishes in a symmetric coupling configuration where $\eta_1 = \eta_2 = 1/2$.

In contrast, the total scattering state $A_{net} = 0$ only demands the intensity condition $I_1/I_2 = \eta_2/\eta_1$ with no restriction on the partial decay rates. In this case,

$$A_{net}(\omega_0) = \frac{4(\gamma_A - \gamma_G)\gamma_{rad}}{\gamma_{rad} + \gamma_A - \gamma_G} 2\eta_1\eta_2 \left[1 + \cos(\phi + \phi_0)\right]. \quad (4)$$

Here, A_{net} vanishes for $\phi + \phi_0 = (2q + 1)\pi$ as a result of destructive interference in the SPP field and consequent null excitation of the resonance mode.

For a critically coupled absorber that has symmetric coupling strength, i.e., $\eta_1 = \eta_2 = 1/2$, the CPA and total scattering states can be obtained simply by switching the phase difference ϕ between $2q\pi–\phi_0$ and $(2q + 1)\pi–\phi_0$ under equal-power incidence ($I_1 = I_2$). In the structure in Fig. 1(a), the external coupling parameters γ_{rad}, η_1, and η_2 are appropriately optimized by tuning the grating depth d and ridge width g that determine the amplitude of the Fourier component for each diffraction order. In addition, the non-radiative decay rate, γ_{nr}, can be finely adjusted by thermally tuning γ_A or optically pumping the PMMA over-layer that controls γ_G.

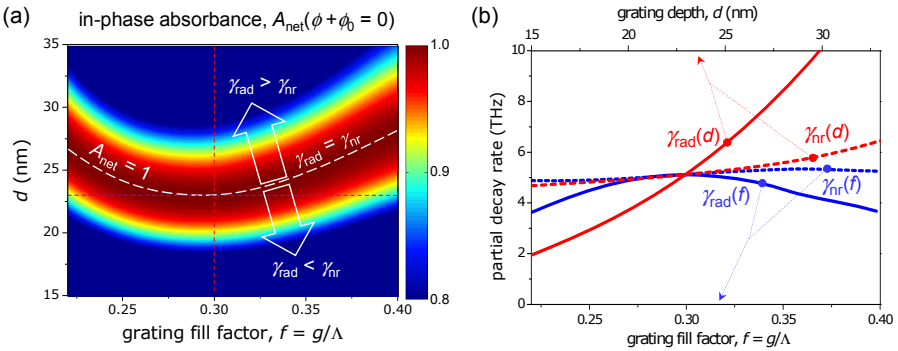

Fig. 2. Geometrical-parameter dependence of the net absorbance and partial decay rates for a specific design with period Λ = 700 nm and PMMA over-layer thickness t = 160 nm. (a) Net in-phase absorbance $A_{net}(\phi + \phi_0 = 0)$ as a function of grating depth d and relative ridge width (fill factor) $f = g/\Lambda$. (b) Partial decay rates γ_{rad} and γ_{nr} as separate functions of d and f. In (b), fill factor is fixed at f = 0.3 for $\gamma_{rad}(d)$ and $\gamma_{nr}(d)$ indicated by the red solid and red dashed curves, respectively, while grating depth is fixed at d = 23 nm for $\gamma_{rad}(f)$ and $\gamma_{nr}(f)$ indicated by blue solid and blue dotted curves, respectively.

As a further step toward experimental study on fine-tuned surface-plasmonic CPA elements, we numerically optimize the structure with a fixed grating period at Λ = 700 nm and PMMA over-layer thickness at t = 160 nm. We use the Chandezon method [15] for numerical calculation. Ag is modeled as a Drude metal with plasma frequency ω_p = 8.01 eV and room-temperature collision frequency Γ_0 = 0.051 eV [16]. The calculated in-phase net absorbance $A_{net}(\phi + \phi_0 = 0)$ in the parametric search space over the range 15 nm ≤ d ≤ 35 nm and 0.22 ≤ g/Λ ≤ 0.4 is shown in Fig. 2(a). In this calculation, we fix vacuum wavelength at 632.8 nm and track the resonance angle θ_m for both coupling diffraction orders m = 1 and 2. Following the derived CPA state condition, intensities I_1 and I_2 of the two incident planewaves are also set such that they satisfy $I_1/I_2 = \eta_1/\eta_2$. Looking at the calculated result in Fig. 2(a), we identify a dashed curve tracing the exact CPA state where A_{net} = 1. The critical coupling condition $\gamma_{rad} = \gamma_{nr}$ is satisfied on these parametric loci. For grating depths smaller than this critical coupling curve, the SPP resonance is under-coupled with $\gamma_{rad} < \gamma_{nr}$. Over-coupled resonance ($\gamma_{rad} > \gamma_{nr}$) occurs in the grating depth region above the critical coupling

#242474 Received 10 Jun 2015; revised 16 Jul 2015; accepted 17 Jul 2015; published 22 Jul 2015

curve. See Fig. 2(b) for the dependence of γ_{rad} and γ_{nr} on grating depth d and fill factor $f = g/\Lambda$. The calculated partial decay rates are found using the method proposed in [17].

The dependence of partial decay rates reveals that γ_{rad} monotonically increases with d but has an upper limit in its f dependence. Therefore, we may utilize d as the main parameter for optimizing γ_{rad} while using f for fine adjustment. In contrast, γ_{nr} is almost independent of d and f because it is dominantly determined by intrinsic properties such as ohmic damping of free electrons in Ag and also the gain coefficient in the dye-doped PMMA over-layer. In particular, a slightly under-coupled resonance ($\gamma_{rad} < \gamma_{nr}$) is desirable for gain-assisted critical coupling where γ_{nr} approaches γ_{rad} by increasing γ_G under optical pumping in the PMMA over-layer. In addition, a slightly over-coupled case ($\gamma_{rad} > \gamma_{nr}$) is appropriate for temperature-tuned critical coupling where thermal heating of the sample enhances free-electron collision in Ag and γ_{nr} increases toward γ_{rad} consequently. We note that temperature or gain tuning does not involve any geometrical parameter changes and thereby provides an experimentally favorable method for accessing the exact critical coupling condition for a given absorber. In the following sections, we describe how we design, fabricate, and characterize the proposed coherent absorbers, as well as experimentally investigate their performances with temperature and gain tuning methods, respectively.

3. Temperature-tuned critical coupling

We fabricate samples for the temperature-tuned CPA experiment using ultraviolet laser holographic lithography and Ar-based reactive ion etching. Under optimal process conditions, we obtain an Ag grating with d = 25 nm, Λ = 720 nm, and f = 0.38 as shown in the AFM image in Fig. 3(a). The grating surface is then spin-coated with a 160-nm-thick PMMA layer without dye doping. Although this experimental device parameter set appears to be under-coupled in the theoretical map in Fig. 2(a), this device in experiments performs in a slightly over-coupled regime. We consider that this inconsistency is due to an incorrect room-temperature collision frequency Γ_0 value which is used to model Ag as a Drude metal in Fig. 2(a). We note that the Drude model is approximate for describing Ag in the visible spectral domain because of the interband electronic transition around 4 eV. The fabricated sample is measured with a two-beam interference set-up schematically illustrated in Fig. 3(b). Two coherent He-Ne laser beams (a_1, a_2) at a vacuum wavelength 632.8 nm are simultaneously incident on the sample surface at resonance angles θ_1 = 7.7° and θ_2 = –50.3°. The intensity ratio I_1/I_2 is adjusted by variable attenuators in both arms, and the initial phase-difference ϕ on the sample surface is controlled by Piezo-electric mirror M_2 in the second arm. The sample is thermally contacted with a voltage-controlled heating plate for temperature control. The heating plate has a linear tuning constant of 2.77 K/V. In the measurement, we apply a 5-minute-long stabilizing time for every 5 K temperature increment. The actual surface temperature T of the sample is measured by a thermocouple.

The dependences of γ_{nr} and γ_{rad} on temperature are experimentally estimated by monitoring the bandwidth of the angular absorbance [3,17]. In this estimation method, the peak absorbance and the total decay rate $\gamma_{tot} = \gamma_{rad} + \gamma_{nr}$ or equivalently full-width at half-maximum (FWHM) of the absorbance peak are measured parameters. The peak absorbance value is used to infer the ratio of γ_{rad}/γ_{nr} and applying this ratio to the measured FWHM values finally yields absolute decay rate values. As shown in Fig. 4(a), the measured γ_{rad} and γ_{nr} are linear with respect to T. A critical coupling condition is found at T_c = 316.8 K (43.8°C) where γ_{nr} and γ_{rad} cross each other. We attributed the linear dependences of γ_{rad} and γ_{nr} with opposite slopes to the thermo-optic effect of PMMA and temperature-dependent collision frequency of free-electrons in Ag. First, the positive slope of 17.09 GHz/K of γ_{nr} is mainly due to the increase in the imaginary term of the Ag dielectric constant with temperature. The imaginary term is proportional to the collision frequency, Γ, of conduction electrons. At the high-temperature limit, where T is much larger than the Debye temperature T_D, which is 195 K for Ag [18], $\Gamma \sim 2T/(3\tau_0 T_D)$ [19], where τ_0 is the characteristic relaxation time due to the isotropic collision process. Therefore, one can assume $\mathrm{Im}[\varepsilon_{Ag}(T)/\varepsilon_{Ag}(T_0)] \approx (T/T_0)$ and consequently

#242474 Received 10 Jun 2015; revised 16 Jul 2015; accepted 17 Jul 2015; published 22 Jul 2015

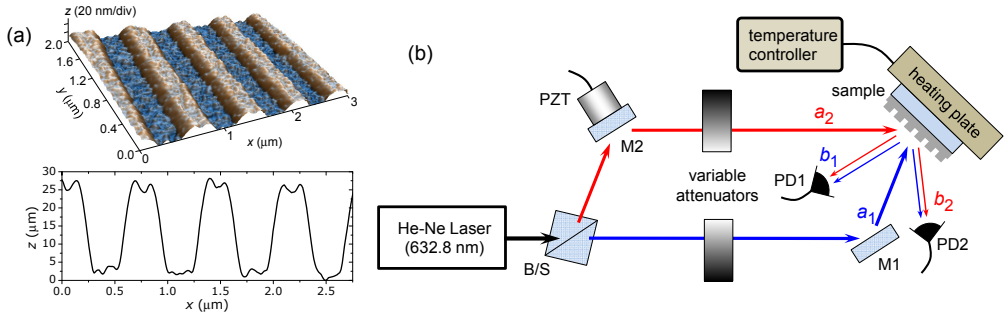

Fig. 3. (a) AFM profile of the fabricated Ag grating and estimated parameters. (b) Schematic of measurement set-up for temperature-tuned CPA measurement.

$$\gamma_{\mathrm{nr}}(T) \approx \frac{T}{T_0}\,\omega \int_{\mathrm{Ag}} \mathrm{Im}\left[\varepsilon_{\mathrm{Ag}}(T_0)\right] |\,\mathbf{E}_{\mathrm{SPP}}\,|^2\, d^3\mathbf{r}, \tag{5}$$

where T_0 is the reference temperature and $\mathbf{E}_{\mathrm{SPP}}$ is a normalized electric field associated with the SPP mode excited on the sample surface.

In contrast, γ_{rad} in Fig. 4(a) linearly decreases with increasing temperature. We attribute this to the normal thermo-optic effect of PMMA with coefficient $\alpha = 3.6 \times 10^{-4}\ \mathrm{K}^{-1}$ for its real dielectric constant [20], i.e., $\mathrm{Re}[\varepsilon_{\mathrm{PMMA}}(T)] = \varepsilon_{\mathrm{PMMA}}(T_0) - \alpha(T - T_0)$. As $\mathrm{Re}[\varepsilon_{\mathrm{PMMA}}(T)]$ decreases with increasing temperature, the evanescent tail of SPP in the PMMA layer becomes longer. Therefore, the portion of modal field energy localized at the Ag grating surface decreases and this effect finally reduces radiation decay of the SPP with increasing temperature.

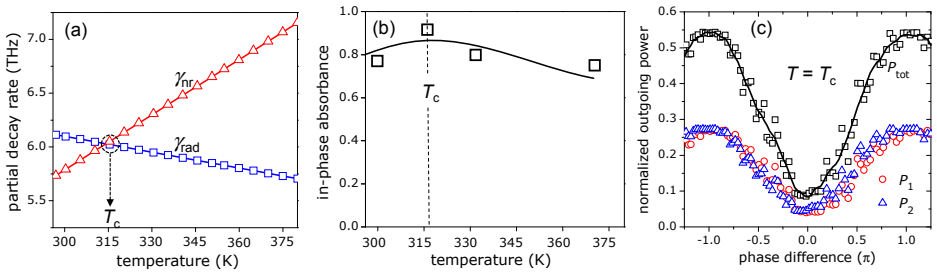

Fig. 4. (a) Measured γ_{nr} and γ_{rad} for the sample showing in Fig. 3(b) as functions of temperature. (b) Measured in-phase net absorbance $A_{\mathrm{net}}(\phi + \phi_0 = 2q\pi)$ as a function of temperature. (c) Measured phase-dependent outgoing powers normalized by the total incoming power. Note that $P_{\mathrm{tot}} = P_1 + P_2$ and the in-phase net absorbance $A_{\mathrm{net}}(\phi + \phi_0 = 2q\pi)$ is taken by the relation $A_{\mathrm{net}}(\phi + \phi_0 = 2q\pi) = 1 - P_{\mathrm{tot}}$ at the P_{tot}-minimum in the phase-dependent outgoing-power measurement.

The net absorbance, A_{net}, measured for the in-phase condition of $\phi + \phi_0 = 2q\pi$ is shown in Fig. 4(b). Among the four sampled temperature values of $T = 300$ K, 316.8 K ($= T_c$), 335 K, and 370 K, we obtain the maximum A_{net} at T_c as expected. The phase-dependent outgoing powers, $P_1 = |b_1|^2$ (red), $P_2 = |b_2|^2$ (blue), and $P_{\mathrm{tot}} = P_1 + P_2$ (black) at $T = T_c$ are shown in Fig. 4(c). Comparing with the theoretical expectations of $A_{\mathrm{net}} = 1$ and $P_{\mathrm{tot}} = 0$ when $\phi + \phi_0 = 2q\pi$, the measured results show an imperfect coherent absorption with $A_{\mathrm{net}} = 1 - P_{\mathrm{tot}} \sim 0.916$. This performance degradation is dominantly due to the non-uniform phase of the incident laser beams that results in non-uniform $\phi + \phi_0$ in the beam cross-section on the sample surface. In addition, small variations in grating period and fill factor over the sample surface may also affect the measured results by introducing an additional non-uniformity in $\phi + \phi_0$.

#242474 Received 10 Jun 2015; revised 16 Jul 2015; accepted 17 Jul 2015; published 22 Jul 2015

4. Gain-assisted critical coupling

In this section, we experimentally study effects of the gain-assisted critical coupling of an SPP-resonant grating. In this experimental analysis, we use Rhodamine-6G (Rh6G) doped in the PMMA over-layer to introduce optical gain in the SPP-resonance region. Optical gain effective to the SPP mode is generally different from that available for bulk photonic modes because of SPP-mediated, position-dependent modification of dye-emission rates [21] and unprofitable emission to lossy surface waves in the nanometric vicinity of the Ag surface [22]. Confirming such an effect in our experimental conditions, we measure photoluminescence spectra of two 1-μm-thick Rh6G-doped PMMA layers separately on bare quartz and Ag-coated (47 nm) quartz substrates as shown in Fig. 5(a). In both cases, the Rh6G-doping concentration is 20 mM. There is remarkable suppression in the spectra for the PMMA layer on Ag in the long wavelength range above 600 nm. This clearly reveals significant modification of the emission properties of Rh6G in the presence of Ag film.

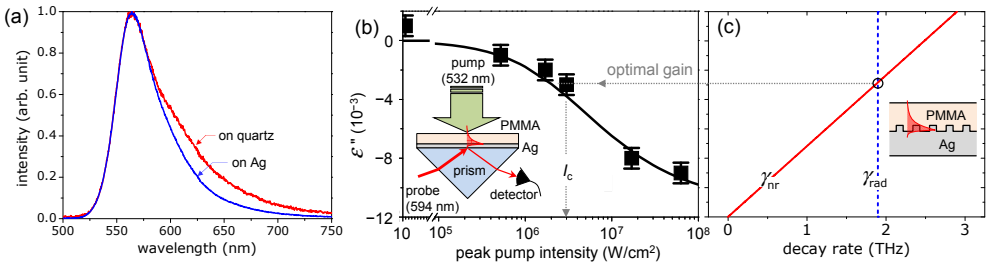

Fig. 5. (a) Modification of photoluminescence on the Ag surface under optical pumping at 532 nm. (b) Measured effective gain coefficient as a function of pumping density. Set-up arrangement for effective gain-coefficient measurement is shown in the inset. We use a 47-nm-thick Ag film and 1-μm-thick PMMA over-layer doped with Rh6G dye at a concentration of 20 mM. (c) Calculated γ_{nr} and γ_{rad} as functions of effective gain coefficient for a structure consisting of a 1-μm-thick PMMA over-layer doped with Rh6G dye at a concentration 20 mM and an Ag grating with a period of 647 nm, fill factor of 0.28, and depth of 18 nm.

We experimentally determine the effective gain coefficient with the classical Kretchmann-Raether configuration shown schematically in the inset in Fig. 5(b). The 1-μm-thick Rh6G-doped PMMA layer on the unpatterned 47-nm-thick Ag film is optically pumped by a pulsed laser beam at a vacuum wavelength of 532 nm, pulse width of 10 ns, and repetition rate of 10 Hz. Angular reflectance of a probe beam at 594 nm is measured with a photodetector with a detection bandwidth of 1 GHz. We fit the measured reflectance data with a standard model based on Fresnel equations to estimate the imaginary dielectric constant, ε", of the Rh6G-doped PMMA layer. Figure 5(b) shows the obtained ε" values in the range from 0.98×10^{-3} to -9.03×10^{-3} as the pump peak intensity, I_p, increases from 0 to 60 MW/cm^2. The corresponding effective gain coefficient, $G = -2\pi\varepsilon"/n\lambda$, covers from –64.9 cm^{-1} at $I_p = 0$ to 597.7 cm^{-1} at $I_p = 60$ MW/cm^2. The experimental values agrees well with the three-level model (solid curve) proposed by Leon et al. [21]. In the model calculation for comparison, we apply an additional small-signal approximation that ignores terms associated with nonlinear gain saturation at high probe field intensity levels.

Figure 5(c) shows the calculated γ_{nr} and γ_{rad} as a function of ε" for the dye-doped PMMA layer on an Ag grating with a period of 647 nm, fill factor of 0.28, and depth of 18 nm. These grating parameters are measured values from a fabricated device. In contrast to γ_{rad} fixed at 1.89 THz, γ_{nr} increases linearly with ε". The crossing point indicating that a critical coupling condition is obtained at $\varepsilon" = -2.8 \times 10^{-3}$ and the corresponding optimal pump intensity I_c found from the experimental data in Fig. 5(b) is ~3 MW/cm^2.

#242474 Received 10 Jun 2015; revised 16 Jul 2015; accepted 17 Jul 2015; published 22 Jul 2015

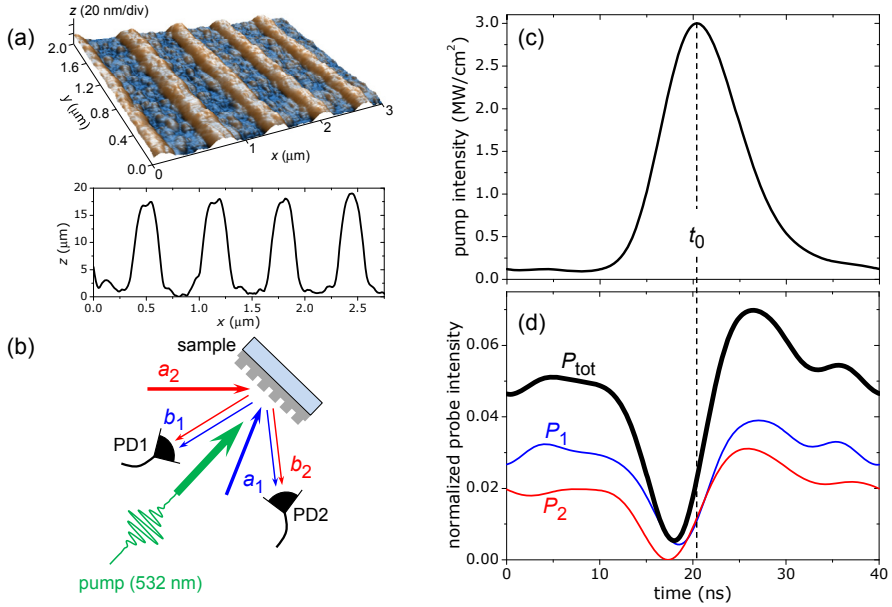

Fig. 6. (a) AFM profile of the fabricated Ag grating and estimated parameters. (b) Schematic of measurement set-up for the temperature-tuned CPA scheme. Measured correlation between (c) pump and (d) coherent probe intensities for the fabricated device. The probe intensity values in (d) are normalized by the total incoming probe power.

Under the optimal pumping at I_c, we finally evaluate coherent absorption properties of the prepared sample shown in Fig. 6(a). The sample supports an SPP resonance at two incidence angles $\theta_1 = 13.2°$ and $\theta_2 = -45.4°$ for probe wavelength 594 nm. The pumping beam at 532 nm with optimal intensity $I_c \sim 3$ MW/cm^2 is normally incident on the sample surface as shown in Fig. 6(b). To improve probe beam's quality with more uniform phase distribution and less beam divergence in this measurement, we employ spatial filtering with a 10-μm-wide pinhole and take the central part of the filtered beam with low numerical aperture collimation lens. We conduct 10 consecutive measurements to average time-resolved pump intensity and probe outgoing powers P_1, P_2, and P_{tot}. Before the main measurements, we prepare interferometer's conditions such that P_{tot} is minimized in the absence of an optical pump. The average pump pulse intensity has a Gaussian shape with a peak at $t_0 = 20.4$ ns as indicated by the vertical dotted line in Fig. 6(c). The slightly longer tail after the peak is due to the detector's response time about 1 ns. Figure 6(d) shows the average outgoing powers of the probe beams normalized by the incoming power. As the pump starts increasing from 10 ns, the outgoing powers P_1, P_2, and P_{tot} decreases even though the optical gain in the PMMA layer increases with pump intensity. P_{tot} is minimized down to 0.00532 of the net incoming intensity at a particular moment $t = 18$ ns. Comparing this P_{tot} minimum with the initial one at $t = 0$ clearly demonstrates the proposed effect of gain-assisted critical coupling with gain-induced enhancement of absorption by a factor 8.7. For $t > 18$ ns, we observe a steep increase in P_{tot} until it reaches its maximum 0.07 at $t = 26.4$ ns. This maximum associated with absorbance minimum is attributed to a pump-induced transient heating effect that increases ohmic absorption in Ag. The transient heating increases γ_{nr} as previously explained in Sec. 3, thereby detuning the absorber from the critical coupling condition.

5. Conclusions

We experimentally demonstrated temperature-tuned and gain-assisted coherent perfect absorption using SPP-resonance gratings. We theoretically investigated parametric optimization of SPP-resonant Ag gratings for generating finely-tuned CPA elements. Temperature-tuned and gain-assisted surface-plasmonic CPA elements were successfully

#242474 Received 10 Jun 2015; revised 16 Jul 2015; accepted 17 Jul 2015; published 22 Jul 2015

created using standard nano-lithography processes, and their performances were tested experimentally. The results clearly show that temperature- and gain-tuning methods are feasible for high-performance CPA elements in practice. The proposed tuning methods are in principle applicable to various CPA configurations including those based on Fabry-Pérot-type optical cavities [1,2], resonant photonic thin films [10,23,24], nanoplasmonic structures [4,7,9], and many others. Therefore, our approach can be considered a general method to obtain high-performance CPAs for future development of compact, low-power, and ultra-fast active optical elements. In addition, incorporation of gain media in dissipative optical systems is presently of great scientific interest to experimentally investigate hypothetical parity-time symmetric quantum mechanics [25] and concomitant optical systems possessing unidirectionality [26] and unconventional mode-selection properties [27]. We expect that our approach can be incorporated in systematic studies on such systems in real experimental platforms.

Acknowledgments

This work was supported in part by the Global Frontier Program through the National Research Foundation of Korea funded by the Ministry of Science, ICT & Future Planning (NRF-2014M3A6B3063708).

#242474 Received 10 Jun 2015; revised 16 Jul 2015; accepted 17 Jul 2015; published 22 Jul 2015